



## Functional retinal imaging using adaptive optics swept-source OCT at 1.6 MHz

MEHDI AZIMIPOUR,<sup>\*,†</sup> JUSTIN V. MIGACZ,<sup>†</sup> ROBERT J. ZAWADZKI, JOHN S. WERNER, AND RAVI S. JONNAL

Vision Science and Advanced Retinal Imaging Laboratory (VSRI), Department of Ophthalmology and Vision Science, UC Davis Eye Center, Sacramento, California 95817, USA

\*Corresponding author: mazimipour@ucdavis.edu

Received 4 September 2018; revised 27 January 2019; accepted 5 February 2019 (Doc. ID 344504); published 5 March 2019

**Objective optical assessment of photoreceptor function may permit earlier diagnosis of retinal disease than current methods such as perimetry, electrophysiology, and clinical imaging. In this work, we describe an adaptive optics (AO) optical coherence tomography (OCT) system designed to measure functional responses of single cones to visible stimuli. The OCT subsystem consisted of a raster-scanning Fourier-domain mode-locked laser that acquires A scans at 1.64 MHz with a center wavelength of 1063 nm and an AO system operating in closed-loop. Analysis of serial volumetric images revealed phase changes of cone photoreceptors consistent with outer segment elongation and proportional to stimulus intensity, as well as other morphological changes in the outer segment and retinal pigment epithelium.** © 2019 Optical Society of America under the terms of the [OSA Open Access Publishing Agreement](#)

<https://doi.org/10.1364/OPTICA.6.000300>

Vision begins when photons are absorbed in the photoreceptor outer segment (OS), initiating the biochemical process of photo-transduction. In blinding retinal diseases like retinitis pigmentosa and age-related macular degeneration, vision is lost when these cells become dysfunctional. Current methods for diagnosing and assessing retinal disease, such as examining the appearance of the retina in clinical images and assessing visual function with clinical exams, are effective after extensive pathological changes, but not in the earliest stages of disease. Adaptive optics (AO) flood imaging [1], conventional optical coherence tomography (OCT) [2–6], and full-field OCT [7] have revealed changes in the photoreceptor OS in response to visible stimuli. Here, we describe an OCT imaging system that leverages the three-dimensional (3D) cellular resolution of AO and OCT [8,9] and the speed of a Fourier-domain mode-locked (FDML) laser [10,11]. This enabled us to resolve cone photoreceptors in three dimensions and characterize changes in single cones OS morphology evoked by impulse-like bleaching flashes.

A schematic of the AO-OCT system is shown in Fig. 1(A). The AO-OCT system consisted of OCT and AO subsystems. The swept-source (SS) OCT system employed a FDML laser

(FDM-1060-750-4B-APC, OptoRes GmbH, Munich, Germany) operating at an A-scan rate of 1.64 MHz [10,11]. A Michelson interferometer with three 50:50 fiber couplers was used to balance spectra of two detection channels. This topology is advantageous in suppressing relative intensity noise (RIN) from the laser [12]. The exposure level of the imaging beam was 1.8 mW, which is below the American National Standards Institute (ANSI) limit for the safe use of lasers, and the measured sensitivity of the system was -85 dB. The sample arm of the system consisted of pairs of spherical mirror telescopes in an out-of-plane configuration [Fig. 1(B)] [13] to correct beam distortions and astigmatism that otherwise accumulate as light is relayed off-axis by multiple in-plane spherical mirrors. The scanning system contained a resonant scanner (SC-30, Electro-Optical Products Corp., Ridgewood, New York) oscillating at 5 kHz in the horizontal direction and a galvanometer scanner in the slower vertical direction. The scanner configuration, in concert with the A-scan rate, permitted acquisition of 32 volumes per second over a field of view of  $1^\circ \times 1^\circ$  (160 A scan per B scan and 160 B scan per each volume). Table 1 summarizes the significant characteristics of the system and data acquisition settings during imaging. The axial resolution of the OCT system was estimated experimentally by placing a flat mirror in place of the subject's eye and measuring the full width at half-maximum (FWHM) of the point spread function (PSF). As is shown in Fig. 2(B), the axial resolution was 10.8  $\mu\text{m}$  in air, which corresponds to 7.8  $\mu\text{m}$  in tissue ( $n = 1.38$ ). Sensitivity roll-off was determined by moving the reference arm while a flat mirror was placed in the sample arm. Based on the roll-off in Fig. 2(C), sensitivity was reduced by 6 dB approximately 2 mm from the zero path length.

The AO subsystem incorporated a Shack-Hartmann wavefront sensor (SHWS) consisting of a  $20 \times 20$  lenslet array (diameter, 10 mm; pitch, 500  $\mu\text{m}$ ;  $f = 30$  mm, Northrop-Grumman Corp, Arlington, Virginia) in front of a scientific complementary metal-oxide-semiconductor (sCMOS) camera (Ace aca2040-180 km; Basler AG), and a high-speed deformable mirror (DM-97-15; ALPAO SAS, Montbonnot-Saint-Martin, France). The wavefront beacon source was a 840 nm superluminescent diode (Superlum Diodes Ltd, Cork, Ireland), with power measured at the cornea of 20  $\mu\text{W}$ . The system measured and corrected aberrations over a 6.75 mm pupil with a closed loop at a rate of 15 Hz, yielding a theoretical lateral resolution of 3.2  $\mu\text{m}$ .

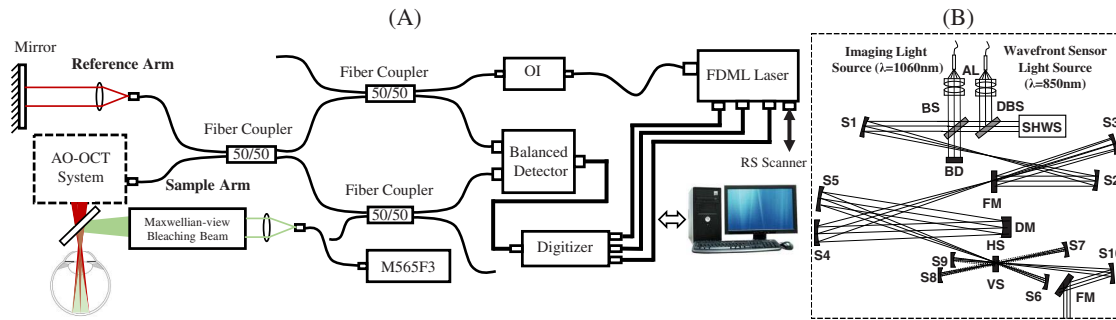


**Fig. 1.** (A) Schematic of the AO-FDML OCT imaging system integrated with Maxwellian-view optical system for bleaching photoreceptors. (B) An expanded view of the AO scanning system: DM, deformable mirror; SHWS, Shack–Hartmann wavefront sensor; AL, achromatic lens; S, spherical mirror; FM, flat mirror; BS, beam splitter; DBS, dichroic beam splitter; HS, horizontal scanner; VS, vertical scanner; BD, beam dump; OI, optical isolator.

**Table 1. Specifications of the AO-FDML System and Scanning Parameters During Imaging**

Laser center wavelength	1063 nm
Spectral bandwidth (FWHM)	78 nm
Laser A-scan rate	1.64 MHz
B-scan rate	5 kHz
Volume rate	32 Hz
Optical power at cornea	1.8 mW
Axial resolution in air	10.8 $\mu\text{m}$
Measured sensitivity	−85.4 dB
Laser phase noise (rms)	2.6 mrad

Custom software controlled the AO [14] and OCT data acquisition, which were developed in Python/Cython and LabVIEW (National Instruments, Austin, Texas), respectively. OCT signal processing was done in MATLAB computing software (The MathWorks, Inc., Natick, Massachusetts) and Python/NumPy/Scipy.

Two subjects, free of known retinal disease, were imaged after obtaining informed consent. Each subject's eye was dilated and cyclopleged by instilling topical drops of 2.5% phenylephrine and 1% tropicamide. All procedures were in accordance with the tenets of the Declaration of Helsinki and were approved by the University of California, Davis Institutional Review Board. To position and stabilize the subject's pupil during imaging, a bite bar and a forehead rest were employed and assembled on a motorized X-Y-Z translation stage. During imaging, a calibrated fixation target was employed to position the eye at specified retinal locations as well as to reduce eye movements. For

functional imaging, subjects were dark-adapted for 15 min and then imaged for 10 s at a retinal location  $2.5^\circ$  temporal to the fovea, where the expected cone row spacing was  $\approx 5.0 \mu\text{m}$  [15]. At the 2 s mark a 10 ms visible flash was delivered. A band-pass filter centered at 555 nm with 20 nm bandwidth was placed in front of the bleaching light source, which was a fiber-coupled LED (M565F3, Thorlabs, New Jersey). This light bleaches *L* and *M* cones almost identically. Flash intensity was modulated in order to bleach between 1.8% and 70% of *L/M* photopigment.

A strip-based registration method [16,17] was implemented to track individual cones in the volume series. First, the volumetric images were segmented axially and the inner segment (IS)/OS and cone OS tip (COST) layers were automatically identified and projected. The *en face* projection of the cone mosaic from a single volume and an average of 30 motion-corrected volumes is shown in Fig. 3. For each series, a single IS/OS projection was selected as a reference image, and the remaining projections were divided into strips of between 5 and 11 pixels of height and registered to the reference. Cones were automatically identified in the reference image. Segmentation and lateral registration together permitted 3D tracking of single cones over time. The time series of the complex axial signal (*M* scans) of each cone were recorded. As the phase of the OCT signal provides a sub-resolution measure of the object's motion [18], we recorded the phase difference between the reflection at IS/OS and COST [17], which provides an estimate of OS length change that is immune to artifacts of axial eye movement:

$$(\Delta\phi)_{t_n} = \angle \left( \frac{1}{m} \sum_{i=1}^m A_i \times B_i^* \right), \quad (1)$$

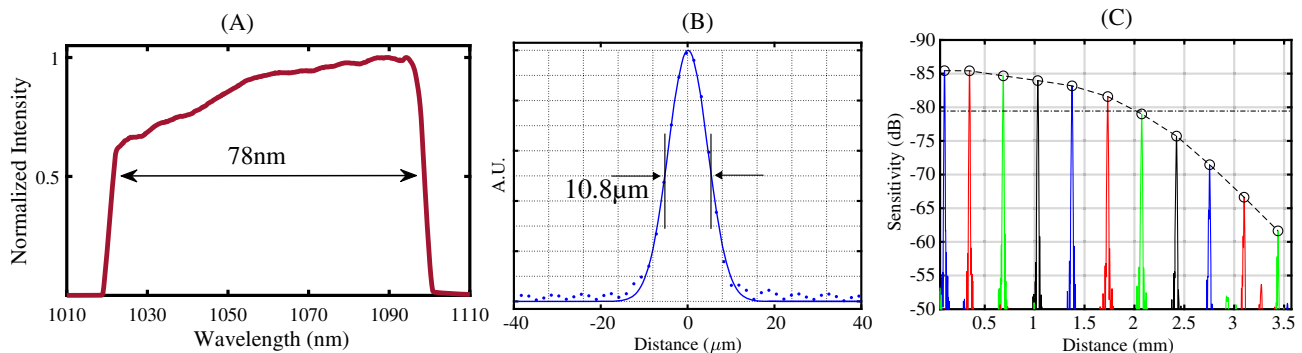


**Fig. 2.** (A) Spectrum of FDML laser. (B) Axial point spread function and (C) sensitivity roll-off of the imaging system.

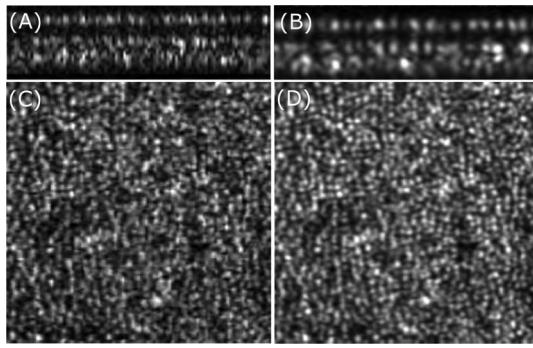


**Fig. 3.** Strip-based registration permits averaging of AO-OCT volumes. Top panel shows (A) single B scan and (B) average of 30 B scans. *En face* projection of cone mosaic from a (C) single and (D) average of 30 motion-corrected volumes of a  $1^\circ$  patch acquired at  $2.5^\circ$  temporal from the foveal center.

where  $A$  is a complex number corresponding to the OCT signal measured at reflection from COST,  $B^*$  is the complex conjugate of the OCT signal measured at reflection from IS/OS, and  $m$  is the number of  $A$  scans recorded within each single cone. After subtracting the initial phase  $\Delta\phi_{t_0}$  from each subsequent measurement and unwrapping the series of phase values, based on the imaging wavelength  $\lambda$ , the change in optical path length  $\Delta\Lambda$  was calculated using

$$\Delta\Lambda_{t_n} = \frac{(\Delta\phi)_{t_n}}{4\pi} \lambda. \quad (2)$$

Observed changes in  $\Lambda$  could be due to changes in the physical length  $L$  of the OS or to changes in its refractive index  $n$ , and the OCT signal's phase cannot distinguish between these. However, investigators have used X-ray diffraction by dissected frog OSs to show that light exposure increases inter-disc spacing by 1%–3% [19]. Thus, we have assumed the change in  $\Lambda$  is due to a change in physical length  $L$ , calculated as  $\Lambda/n$  with  $n = 1.38$ , which is what is shown in the plots. A response of a single cone to a 70% photopigment bleaching flash is shown in Fig. 4(A). *En face* projections of the cone's neighborhood are shown at the top. Next, the amplitude of the cone's  $M$  scan is shown, with the stimulus flash

indicated by a green line. Changes in the cone's axial profile subsequent to the flash are visible: the IS/OS reflectivity decreases, the distance between COST and IS/OS appears to increase, and structural changes are visible in other layers. At the bottom, the phase difference between IS/OS and COST is shown as a function of time. Responses of cones to three different flash intensities are shown in Fig. 4(B). Each response is the OS elongation corresponding to the measured phase difference between IS/OS and COST. It is apparent that the magnitude of elongation varies with stimulus strength, as does the time required for the cone to recover its baseline length. This observed elongation of foveal/parafoveal cones, and the dependence of elongation on stimulus intensity, is qualitatively consistent with previously reported elongation of peripheral cones using full-field OCT with computational aberration correction [7]. We hypothesize that the mechanism of this elongation is osmotic swelling of the OS, as it is consistent with observations made using conventional OCT images in human rods [5] and mouse rods, in which elongation is suppressed in mice lacking transducin [20].

In addition to OS elongation, changes in axial morphology were often observed subsequent to the stimulus flash. Representative  $M$  scans of single cones for photopigment bleaching percentages of 1.8, 7, and 70 are shown in Fig. 5. A common observation was the appearance and/or movement of an extra band between IS/OS and COST, indicated by red arrows in Fig. 5. The reflectivity of this band and its maximal axial distance from IS/OS appear to be proportional to the bleaching light intensity, and it is most evident in the 70% bleaching trials (5 C), where it moves half the length of the OS within 1–2 s. Generally, OCT signals are attributed to refractive index mismatch, and the movement of this band is consistent with the movement of a refractive index boundary. Such a boundary could be generated, for instance, by an abrupt change in disc spacing or concentration of a visual cycle intermediate. The observation is also consistent with coherent effects of modulation in disc spacing [20]. Another common observation was a change in the appearance of the space distal to COST, including the subretinal space (SRS) and retinal pigment epithelium (RPE). The RPE band appears to split, with its apical portion moving inward, toward COST. If melanosomes are an important source of RPE scattering [21], the observed

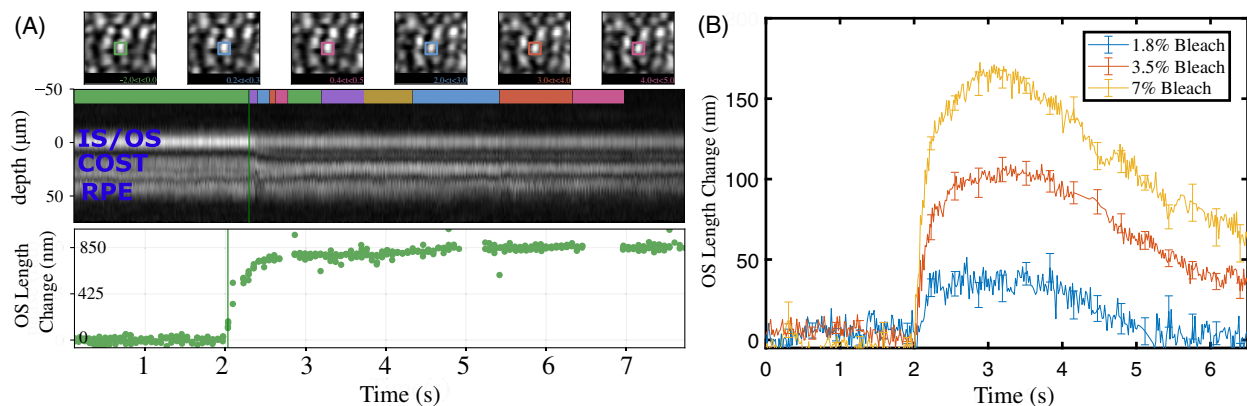


**Fig. 4.** (A) Response of a single cone to 70% photopigment bleaching stimuli. The top row shows examples of motion-corrected *en face* projections of the cone's neighborhood. A time series of the cone's axial profile ( $M$  scan) is shown below the *en face* projections, with a green line indicating the stimulus flash. The phase difference between the IS/OS and COST was monitored as a function of time and can be seen in the bottom plot. (B) OS length change as a function of time for lower  $L/M$  photopigment bleaching percentages of 1.8, 3.5, and 7. Each curve was produced by averaging responses of 10–30 cones. Error bars indicate  $\pm$  one standard deviation.

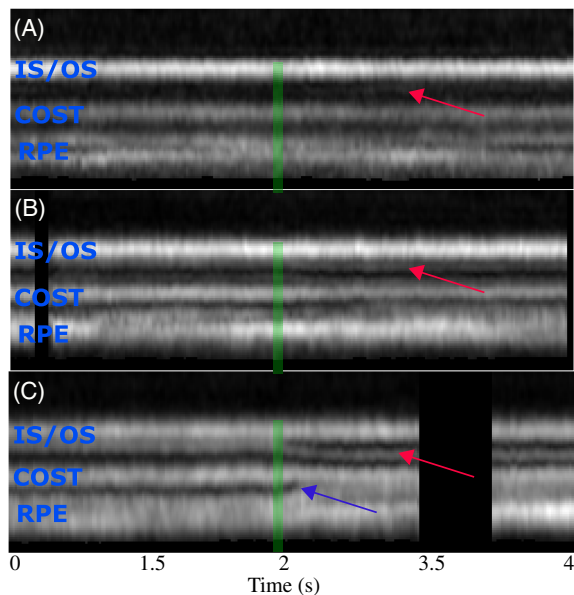


**Fig. 5.** Changes in the axial morphology of cones for photopigment bleaching percentages of (A) 1.8, (B) 7, and (C) 70. As shown by red arrows, appearance of an extra band between IS/OS and COST was observed in most of the cones. The reflectivity of this extra band and also its axial distance from IS/OS seems to be proportional to the bleaching light intensity. The blue arrow indicates changes observed in the RPE and SRS.

movement could be an indication of melanosome movement into the apical part of the RPE cell. This is consistent with light-driven translocation of melanin observed in amphibians [22] but not previously reported in mammals. It may also be a consequence of inward water movement across the Bruchs RPE complex.

A critical feature of this system's design is its speed. For the most intense stimuli, we observed initial phase changes of up to 50 rad/s. In order to correctly unwrap the phase, the phase change between consecutive samples should be less than  $\pi$  radians. This suggests that the minimal rate at which cones must be imaged, i.e., the minimal volume rate, is 16 Hz. In the presence of noise, it is likely that a higher rate is required. Our volume rate of 32 Hz proved sufficient for measuring these fast changes. Another benefit of high-speed acquisition is the reduction of intraframe eye movement artifacts, which permits better registration of frames and tracking of cones.

We have demonstrated that AO-OCT may be used to detect and measure functional responses of foveal cone photoreceptors. It reveals stimulus-evoked OS phase changes, consistent with OS elongation, similar to those previously detected in foveal cones using AO flood illumination and peripheral cones using full-field SS-OCT, and consistent with elongation observed in human and mouse rods. In addition, our images reveal stimulus-evoked changes in the intensity and organization of the outer retinal

bands. These functional responses together represent a rich set of biomarkers of photoreceptor function.

**Funding.** National Eye Institute (NEI) (R01-EY-024239, R00-EY-026068, R01-EY-026556, P30-EY012576).

**Acknowledgment.** The authors acknowledge the assistance of Susan Garcia. R. S. J., J. S. W., and R. J. Z. acknowledge the support from NEI.

<sup>†</sup>These authors contributed equally to this Letter.

## REFERENCES

1. R. S. Jonnal, J. Rha, Y. Zhang, B. Cense, W. Gao, and D. T. Miller, *Opt. Express* **15**, 16141 (2007).
2. V. Srinivasan, Y. Chen, J. Duker, and J. Fujimoto, *Opt. Express* **17**, 3861 (2009).
3. M. D. Abramoff, R. F. Mullins, K. Lee, J. M. Hoffmann, M. Sonka, D. B. Critser, S. F. Stasheff, and E. M. Stone, *Invest. Ophthalmol. Visual Sci.* **54**, 3721 (2013).
4. Y. Li, R. Fariss, J. Qian, E. Cohen, and H. Qian, *Invest. Ophthalmol. Visual Sci.* **57**, 105 (2016).
5. C. D. Lu, B. Lee, J. Schottenhamml, A. Maier, E. N. Pugh, and J. G. Fujimoto, *Invest. Ophthalmol. Visual Sci.* **58**, 4632 (2017).
6. B. A. Berkowitz, R. H. Podolsky, H. Qian, Y. Li, K. Jiang, J. Nellissery, A. Swaroop, and R. Roberts, *Invest. Ophthalmol. Visual Sci.* **59**, 5957 (2018).
7. D. Hillmann, H. Spahr, C. Pfäffle, H. Sudkamp, G. Franke, and G. Hüttmann, *Proc. Natl. Acad. Sci. USA* **113**, 13138 (2016).
8. Y. Zhang, J. Rha, R. S. Jonnal, and D. T. Miller, *Opt. Express* **13**, 4792 (2005).
9. R. Zawadzki, S. Jones, S. Olivier, M. Zhao, B. Bower, J. Izatt, S. Choi, S. Laut, and J. Werner, *Opt. Express* **13**, 8532 (2005).
10. R. Huber, M. Wojtkowski, and J. G. Fujimoto, *Opt. Express* **14**, 3225 (2006).
11. T. Klein, W. Wieser, C. M. Eigenwillig, B. R. Biedermann, and R. Huber, *Opt. Express* **19**, 3044 (2011).
12. Y. Chen, D. M. de Bruin, C. Kerbage, and J. F. de Boer, *Opt. Express* **15**, 16390 (2007).
13. S.-H. Lee, J. S. Werner, and R. J. Zawadzki, *Biomed. Opt. Express* **4**, 2508 (2013).
14. R. S. Jonnal, O. P. Kocaoglu, R. J. Zawadzki, S.-H. Lee, J. S. Werner, and D. T. Miller, *Invest. Ophthalmol. Visual Sci.* **55**, 7904 (2014).
15. C. Curcio, K. Sloan, R. Kalina, and A. Hendrickson, *J. Comp. Neurol.* **292**, 497 (1990).
16. S. Stevenson and A. Roorda, *Proc. SPIE* **5688**, 145 (2005).
17. R. S. Jonnal, O. P. Kocaoglu, Q. Wang, S. Lee, and D. T. Miller, *Biomed. Opt. Express* **3**, 104 (2012).
18. M. A. Choma, A. K. Ellerbee, C. Yang, T. L. Creazzo, and J. A. Izatt, *Opt. Lett.* **30**, 1162 (2005).
19. M. Chabre and A. Cavaggioni, *Nature* **244**, 118 (1973).
20. P. Zhang, R. J. Zawadzki, M. Goswami, P. T. Nguyen, V. Yarov-Yarovoy, M. E. Burns, and E. N. P. Jr, *Proc. Natl. Acad. Sci. USA* **114**, 2937 (2017).
21. E. Götzinger, M. Pircher, W. Geitzenauer, C. Ahlers, B. Baumann, S. Michels, U. Schmidt-Erfurth, and C. K. Hitzenberger, *Opt. Express* **16**, 16410 (2008).
22. Q.-X. Zhang, R.-W. Lu, J. D. Messinger, C. A. Curcio, V. Guarcello, and X.-C. Yao, *Sci. Rep.* **3**, 2644 (2013).